

Supplementary Information

Freestanding cathode with vertically arranged microchannels via phase inversion for quasi-solid-state lithium metal batteries

Yitong Liang^{1, †}, Nan Zhang^{1, †}, Qiwen Chen¹, Shaoping Wu², Hezhou Liu¹, Huanan Duan^{1,*}

¹ State Key Laboratory of Metal Matrix Composites, School of Materials Science and Engineering, Shanghai Jiao Tong University, Shanghai, 200240, P. R. China

² Innovation Laboratory for Sciences and Technologies of Energy Materials of Fujian Province (IKKEM), Xiamen, 361024, P. R. China

[†] These authors contribute equally to this work.

* Corresponding author, Email address: hd1@sjtu.edu.cn

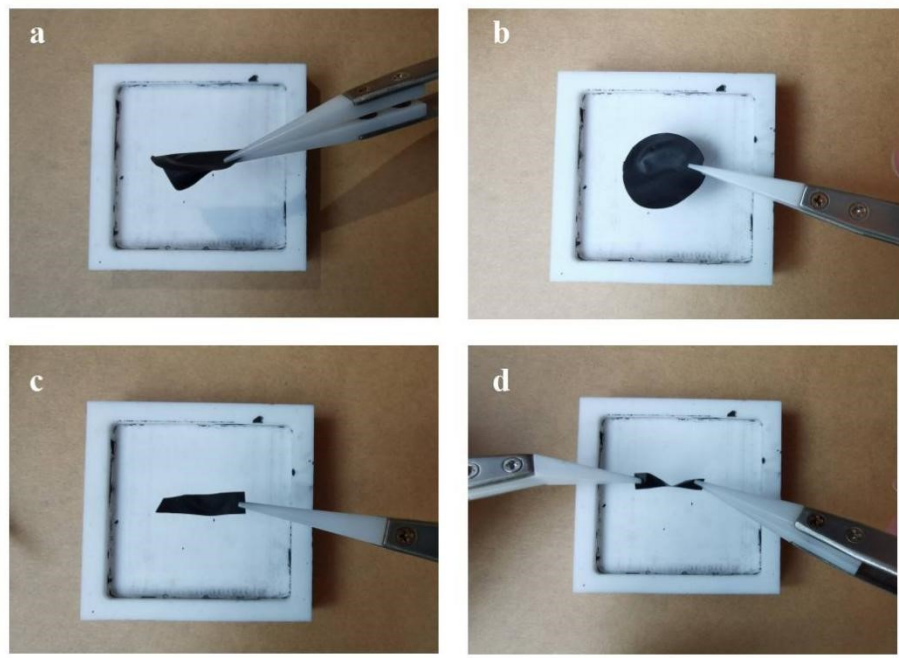


Fig. S1 Digital image of the phase inversion freestanding electrode. The electrode is flexible and twistable.

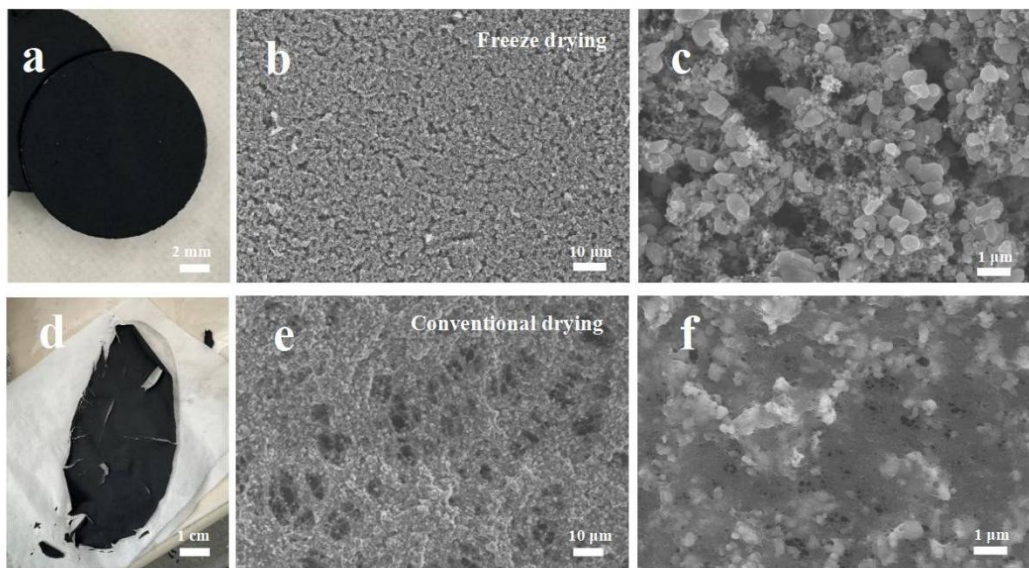


Fig.S2 Digital and SEM images of (a-c) freeze-drying phase inversion cathodes, and (d-f) conventional drying cathodes.

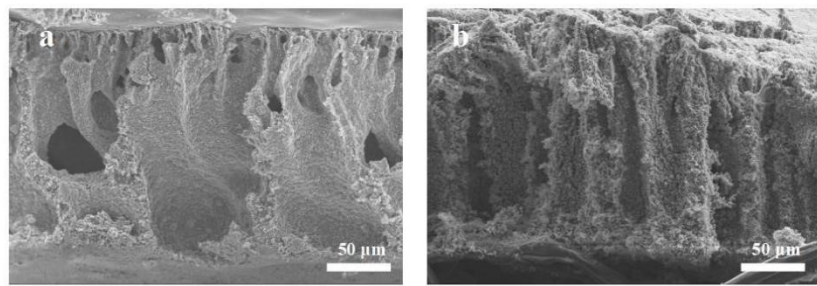


Fig. S3. Side view images of phase inversion cathode with (a) conventional drying at 80 °C and (b) freeze drying at -30 °C.

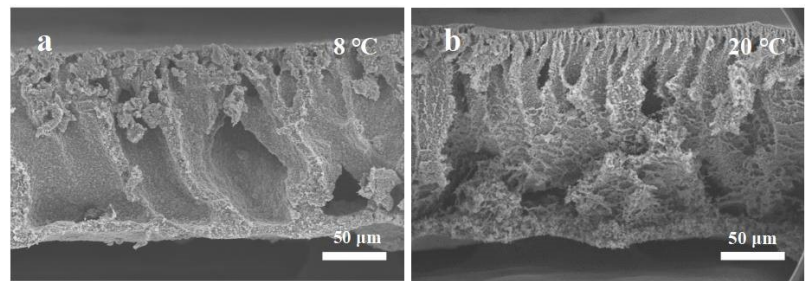


Fig. S4 Side view images of phase inversion cathode with solvent temperature at (a) 8 °C and (b) 20 °C.

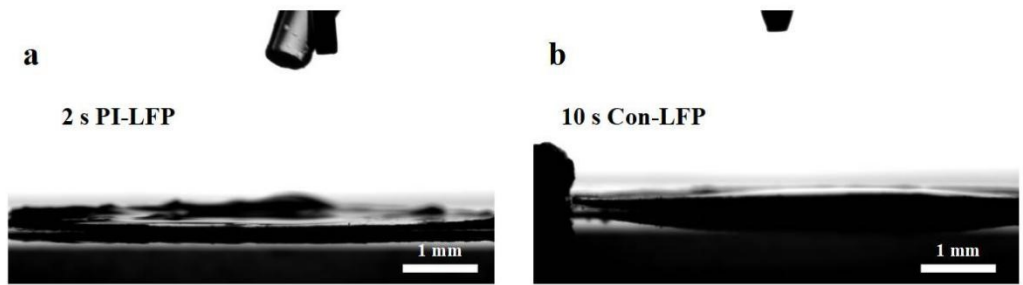


Fig. S5 The time required for the electrode to fully absorb the electrolyte. (a) 2 s for PI-LFP and (b) 10 s for Con-LFP.

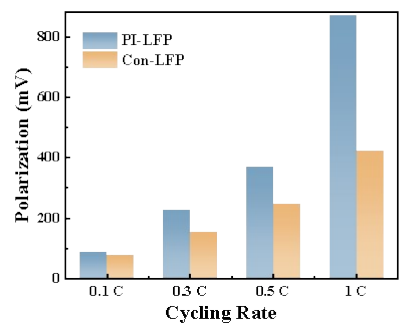


Fig. S6 Summary of the polarization of Li/LFP cell during cycling test.

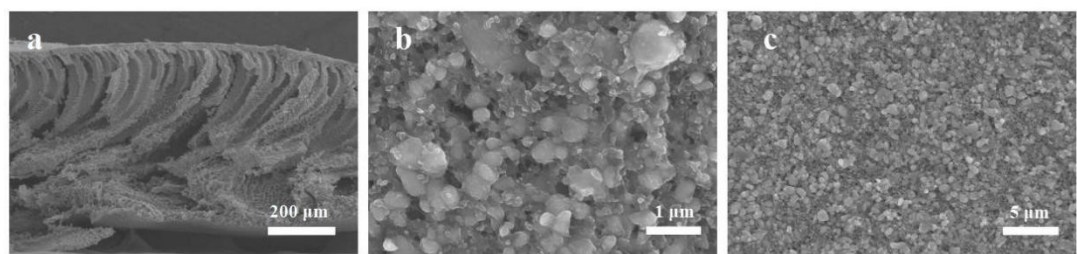


Fig. S7 (a) Side view image of PI-LFP-HL. (b) Top view image of the PI-LFP-HL at 20000 \times . (c) Top view image of the PI-LFP-HL at 5000 \times .

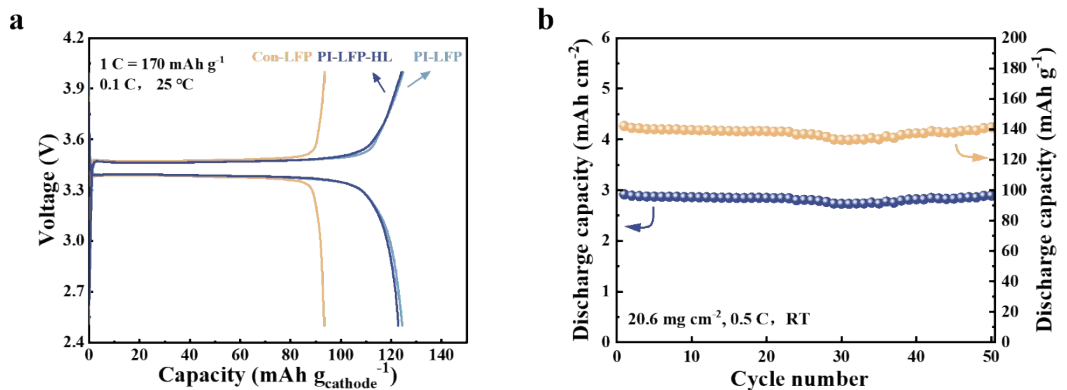


Fig. S8 (a) Specific discharge capacity of Con-LFP (9.5 mg cm⁻²), PI-LFP (9.5 mg cm⁻²), and PI-LFP-HL (20.6 mg cm⁻²) calculated based on the total mass of the cathode. (b) The cycling performance of PI-LFP cathode with a mass loading of 20.6 mg cm⁻² at 0.5 C.

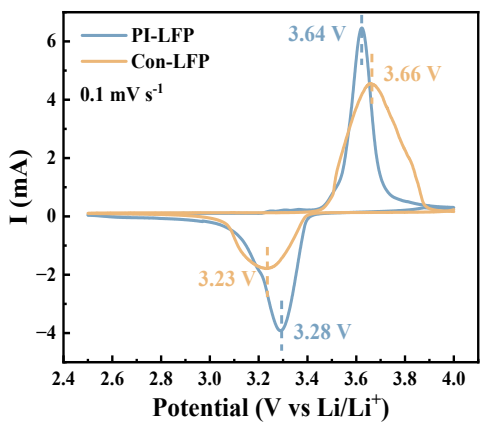


Fig. S9 CV curves of the PI-LFP and Con-LFP cathodes with DOL electrolyte.

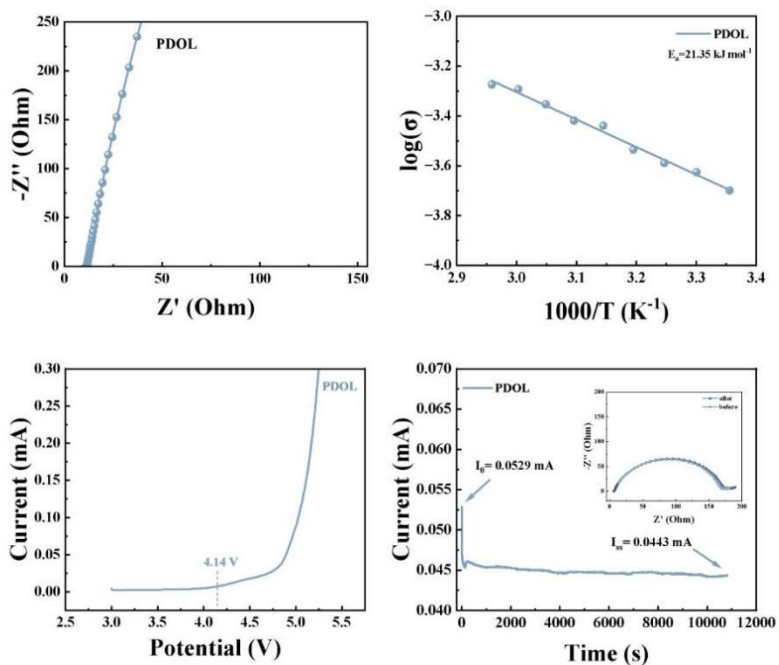


Fig. S10 Basic properties of PDOL gel electrolyte. (a) Ionic conductivity at room temperature. (b) The activation energy of PDOL gel electrolyte. (c) LSV result of PDOL electrolyte. (d) Chronoamperometry test of the symmetric Li|PDOL|Li cell under a polarization voltage of 10 mV, and the insert shows the EIS impedance spectra of the symmetric cell before and after polarization.

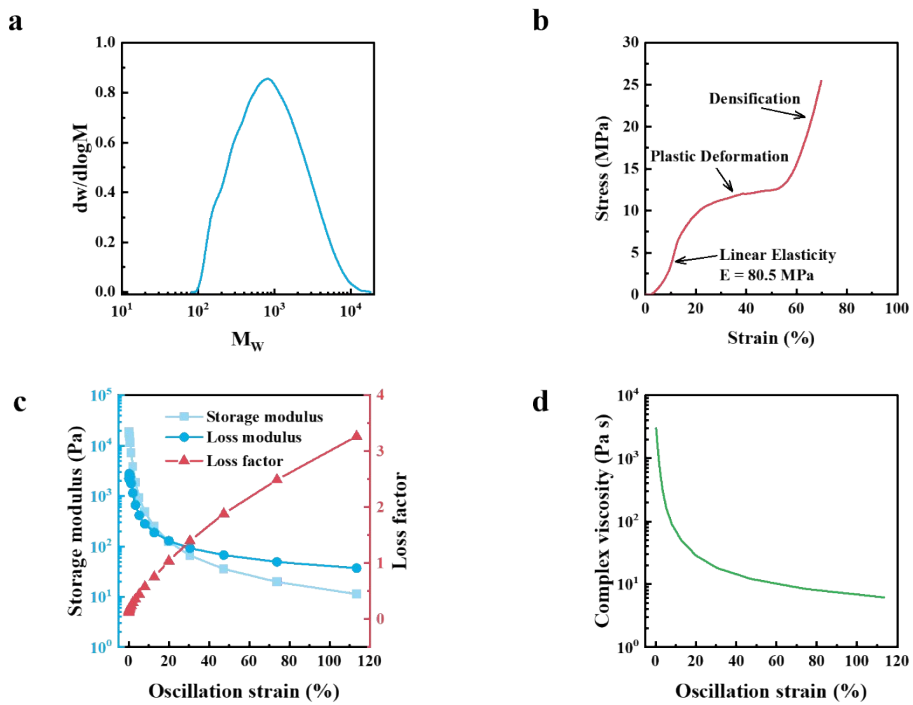


Fig. S11 The molecular weight and mechanical strength of the polymerized PDOL. (a) Molecular weight distribution curve of PDOL; (b) The stress-strain curve of PDOL; (c) The relationship between storage modulus, loss modulus, loss factor, and oscillation strain of PDOL; (d) The complex viscosity curves of PDOL.

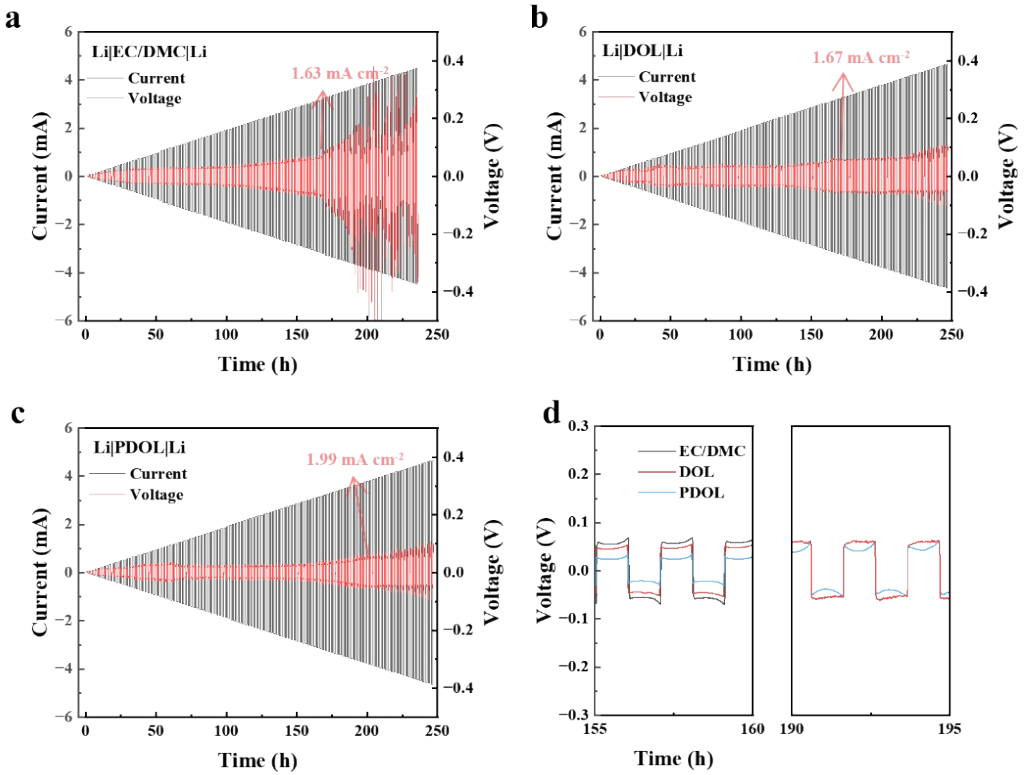


Fig. S12 Time-controlled critical current density (CCD) measurement of the symmetric cells with different electrolytes. (a) EC/DMC; (b) DOL; (c) PDOL; (d) Voltage change of the electrolyte from 155 to 160 h, and from 190 to 195 h.

Note: carbonate-based electrolyte, DOL and PDOL has a critical current density as 1.63, 1.67 and 1.99 mA cm⁻², respectively. The carbonate electrolyte has the largest polarization, followed by the DOL-based and PDOL-based electrolyte. Partly short circuit can be identified when the sudden voltage change happens¹, indicating the change of internal resistance. PDOL has a higher CCD value, which can be attributed to the enhanced mechanical robustness. It has a significant impact on the suppression of lithium whiskers². Therefore, the PDOL gel electrolyte provides better safety performance compared with liquid electrolyte.

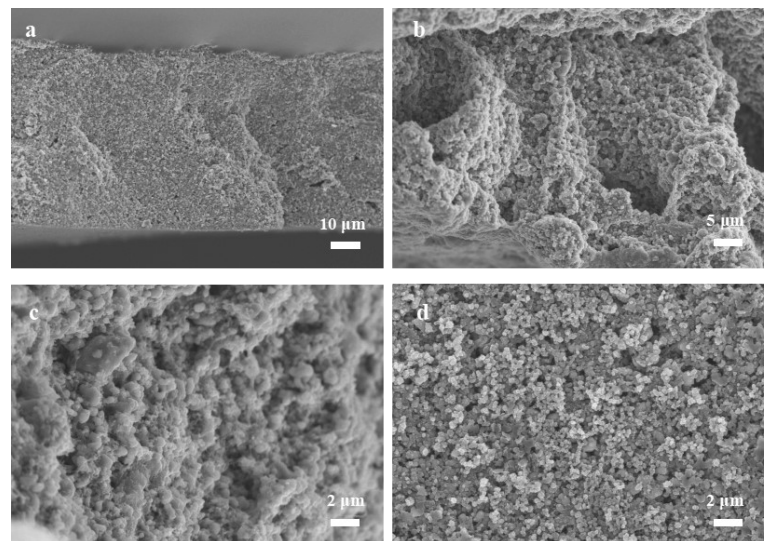


Fig. S13 SEM figure of PI-LFP after 50 cycles at 0.5 C. Side view images of PI-LFP at 1000×; (b) 2000×; (c) 5000×. (d) Top view image of the PI-LFP electrode at 5000×.

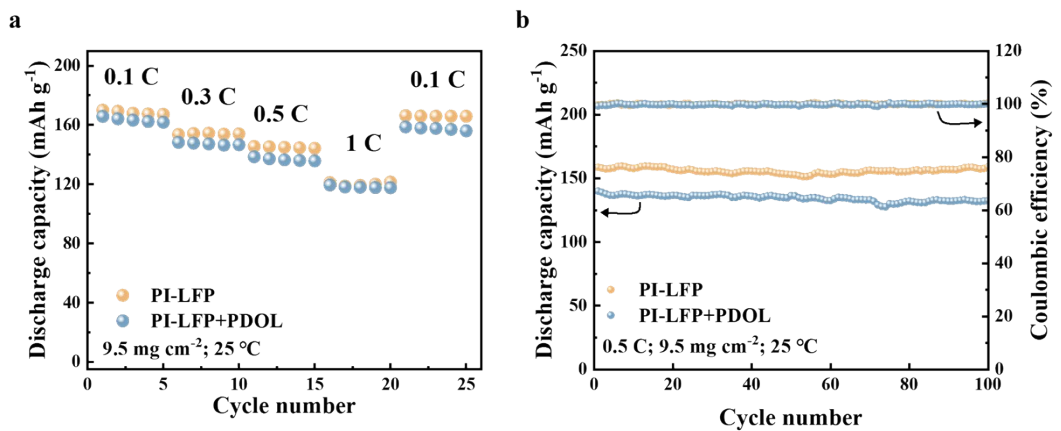


Fig.S14 The comparison of PI-LFP+PDOL and PI-LFP electrode with active material loading as 9.5 mg cm^{-2} . (a) Rate performance; (b) cycling performance.

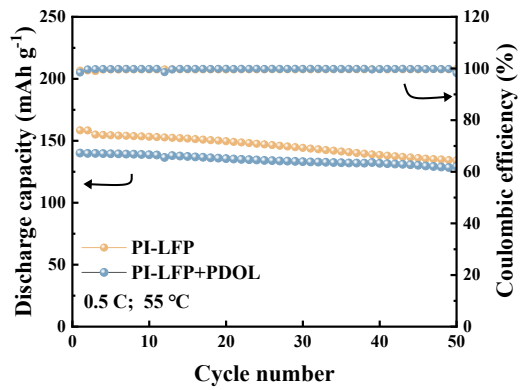


Fig. S15 Cycling performance of PI-LFP+PDOL and PI-LFP electrode at 55 °C.

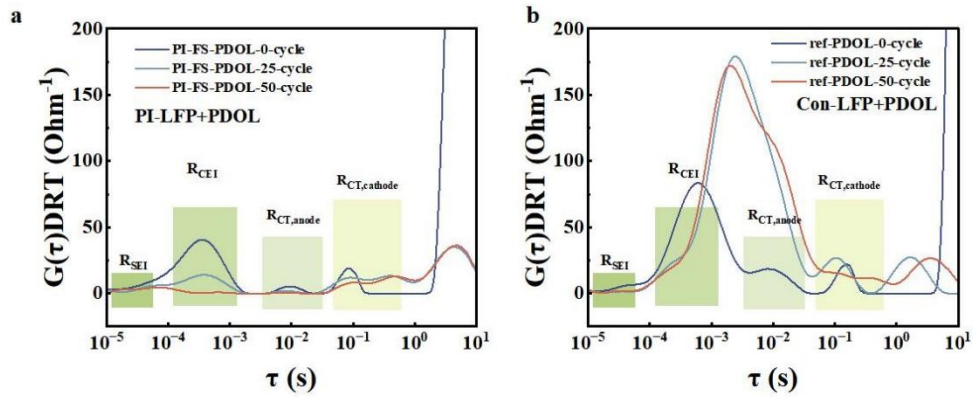


Fig. S16 R_{SEI} , R_{CEI} and R_{CT} from DRT analysis of different cycle numbers at 0.5 C. (a) PI-LFP+PDOL, (b) Con-LFP+PDOL.

Table S1 The mass ratio of the composition of PI-LFP and Con-LFP at 9.5 mg cm⁻².

No.	Cathode	Composition of the slurry			
		Conducive	Binder/	Active	Current
		agent	dispersant	material	collector
1	PI-LFP	13.5%	14.4%	72.1%	--
2	Con-LFP	8.3%	8.3%	66.5%	16.8%

Table S2 Summary of the basic properties of PDOL gel electrolyte.

Basic properties	Ionic conductivity	Activation energy	Oxidation potential	Transference number
PDOL gel electrolyte	1.98×10^{-4} S cm ⁻¹	E _a = 0.230 eV	4.14 V	t _{Li+} = 0.56

Table S3 Comparison of traditional carbonate electrolyte, ether-based electrolyte and this work in lithium metal batteries system.

				Voltage (V vs. Li/Li ⁺)	Loading (mg cm ⁻²)	Dischargeg rate (C)	Cycle number	Capacity retention	Initial discharge capacity (mAh g ⁻¹)
	Ref	Battery type	Electrolyte						
	3	Li/LFP	1 M LiPF ₆ +EC/DMC	2.8–4.0	6	0.5	130	64.3%	~140
	4	Li/LFP	1 M LiPF ₆ +EC /EMC	2.5–4.2	-	1	200	81.6%	125
Carbonate electrolyte	5	Li/LFP	1 M LiPF ₆ +EC/DEC	2.5–4.2	4.2	0.5	100	86.0%	150
	6	Li/LFP	1 M LiTFSI +FEC/DMC	2.5–4.2	12	0.5	210	88.8%	~150
	7	Li/LFP	1 M LiPF ₆ +EC/DMC	2.0–4.0	5	0.5	200	73.3%	~150
	8	Li/LFP	1 M LiPF ₆ +FEC/EC/DEC	2.8-3.8	14.1	0.5	130	51.8%	156.7
	9	Li/LFP	1 M LiFSI + DEE	2.7-4.0	5.83	0.5	200	93.5%	140
	10	Li/LFP	1 M LiTFSI +DOL/DME with 1% LiNO ₃	2.5-3.8	11.76	1	230	72.9%	~140
Ether-based electrolyte	11	Li/LFP	1M LiTFSI +DOL/DME	2.5-4.2	8	0.5	200	60.4%	142.4
	12	Li/LFP	1.0 M LiTFSI+DOL/DME with 5 wt% TMS-	2.75-3.8	4	0.2	100	92.3%	~145
			FNFSI						
This		Li/LFP	1 M	2.5-4.0	9.5	0.5	250	96.3%	~160

work	LiTFSI+DOL/DME							
This work	Li/LFP work	1 M LiTFSI+PDOL/DME	2.5-4.0	9.5	0.5	100	94.7%	140

EC: ethylene carbonate; DEC: diethyl carbonate; FEC: fluoroethylene carbonate; DOL:1,3-dioxolane; DME:1,2-dimethoxyethane; DEE:1,2-diethoxyethane; TMS-FNFSI:(CH₃)₃Si-N[(FSO₂)(*n*-C₄F₉SO₂)]; LFP: LiFePO₄

Table S4 Comparison of PDOL and references as GPE in Li/LFP system.

Ref	Polymerization type	Electrolyte	Voltage Loading		Discharging rate (C)	Cycle number	Capacity retention	Initial discharge capacity (mAh g ⁻¹)
			(V vs. Li/Li ⁺)	(mg cm ⁻²) ²⁾				
13	Ex-situ	1 M LiTFSI+ PVDF-HFP/PEGDME	2.7-3.8	6-7	0.1	60	98%	~148
Other GPE 14	AIBN initiator	1 M LiPF6 +EC/DMC+PEGDA	2.5-4.0	1.5	0.5	100	87.3%	138.6
15	Ex-situ	1 M LiTFSI+PEGDA /DME/TEP with TiO ₂	2.8-4.0	-	0.2	200	85.3%	125.7
9	Y(SO ₃ CF ₃) ₃ initiator	1 M LiTFSI +PDOL+LLZTO	2.8-3.8	1	0.2	200	70%	135
16	Al(OTf) ₃ Initiator	1 M LiTFSI+PDOL	-	5	0.2	200	76.9%	130
PDOL-based GPE		1 M LiTFSI, 1 M LiPF ₆ initiator	2.5-3.7	15	0.5	200	91.8%	151.8
NF								
This work	PAMPS intiator	1 M LiTFSI+PDOL/DME	2.5-4.0	9.5	0.5	100	94.7%	140

PI NF: polyimide nanofiber; LLZTO: Li_{6.4}La₃Zr_{1.4}Ta_{0.6}O₁₂; PEGDA: polyethylene glycol diacrylate; AIBN: 2,2'-Azobis (2-methylpropionitrile); PAMPS: Poly(2-Acrylamido-2-Methyl-1-Propanesulfonic Acid); PVDF-HFP: poly(vinylidene fluoride-co-hexafluoropropylene); PEGDME: poly(diethylene glycol diglycidyl ether)

$$\varepsilon = \frac{\rho_0 - \rho}{\rho_0} = 1 - \rho \left(\frac{\omega_{am}}{\rho_{am}} + \frac{\omega_{ca}}{\rho_{ca}} + \frac{\omega_b}{\rho_b} \right) \#S1$$

ρ_0 and ρ are the active layers' theoretical and measured tap densities, respectively. ω_{am} , ω , ω_b and ρ_{am} , ρ_{ca} , ρ_b are the mass fractions and densities of active material, conductive agent, and binder, respectively.

$$\varepsilon = \frac{4}{\pi \Delta \tau} \left(\frac{m_B V_M}{M_B S} \right)^2 \left(\frac{\Delta E_s}{\Delta E_\tau} \right)^2 \#S2$$

$\Delta \tau$ represents the duration of the applied pulse current, and m_B , M_B , and V_M are the mass, molar mass, and molar volume, respectively. S denotes the contact area, while ΔE_s and ΔE_τ correspond to the voltage changes during one cycle of the pulse current and the voltage changes induced by galvanostatic charging for a certain period, respectively. In the calculation, $V_M = 46 \text{ cm}^3 \text{ mol}^{-1}$, $M_B = 157.76 \text{ g mol}^{-1}$.

Notes and references

1. Y. Lu, C.-Z. Zhao, H. Yuan, X.-B. Cheng, J.-Q. Huang and Q. Zhang, *Advanced Functional Materials*, 2021, **31**, 2009925.
2. H. Yang, M. Jing, L. Wang, H. Xu, X. Yan and X. He, *Nano-Micro Letters*, 2024, **16**, 1-33.
3. C. Yan, Y.-X. Yao, X. Chen, X.-B. Cheng, X.-Q. Zhang, J.-Q. Huang and Q. Zhang, *Angewandte Chemie International Edition*, 2018, **57**, 14055-14059.
4. F. Li, Y. Gong, G. Jia, Q. Wang, Z. Peng, W. Fan and B. Bai, *Journal of Power Sources*, 2015, **295**, 47-54.
5. R. Xu, X.-Q. Zhang, X.-B. Cheng, H.-J. Peng, C.-Z. Zhao, C. Yan and J.-Q. Huang, *Advanced Functional Materials*, 2018, **28**, 1705838.
6. Z. Zhu, Z. Liu, R. Zhao, X. Qi, J. Ji, F. Yang, L. Qie and Y. Huang, *Advanced Functional Materials*, 2022, **32**, 2209384.
7. C. Tao, T. Zheng, P. Jia, W. Gong, G. Yila, L. Wang and T. Liu, *ACS Applied Materials & Interfaces*, 2024, **16**, 23325-23333.
8. Z. Guo, X. Song, Q. Zhang, N. Zhan, Z. Hou, Q. Gao, Z. Liu, Z. Shen and Y. Zhao, *ACS Energy Letters*, 2022, **7**, 569-576.
9. T. D. Pham and K.-K. Lee, *Small*, 2021, **17**, 2100133.
10. G. Zhang, X. Deng, J. Li, J. Wang, G. Shi, Y. Yang, J. Chang, K. Yu, S.-S. Chi, H. Wang, P. Wang, Z. Liu, Y. Gao, Z. Zheng, Y. Deng and C. Wang, *Nano Energy*, 2022, **95**, 107014.
11. X. Fu, X. Deng, Y. Deng, X. Xiong, Y. Zheng, Z. Zhang, D. Dang and G. Wang, *Energy & Fuels*, 2022, **36**, 11219-11226.
12. B. Tong, J. Wang, Z. Liu, L. Ma, P. Wang, W. Feng, Z. Peng and Z. Zhou, *Journal of Power Sources*, 2018, **400**, 225-231.
13. J. Castillo, A. Santiago, X. Judez, I. Garbayo, J. A. Coca Clemente, M. C. Morant-Miñana, A. Villaverde, J. A. González-Marcos, H. Zhang, M. Armand and C. Li, *Chemistry of Materials*, 2021, **33**, 8812-8821.
14. S. Z. Zhang, X. H. Xia, D. Xie, R. C. Xu, Y. J. Xu, Y. Xia, J. B. Wu, Z. J. Yao, X. L. Wang and J. P. Tu, *Journal of Power Sources*, 2019, **409**, 31-37.
15. J. Guo, Y. Chen, Y. Xiao, C. Xi, G. Xu, B. Li, C. Yang and Y. Yu, *Chemical Engineering Journal*, 2021, **422**, 130526.
16. Q. Zhao, X. Liu, S. Stalin, K. Khan and L. A. Archer, *Nature Energy*, 2019, **4**, 365-373.
17. Y. Huang, S. Liu, Q. Chen, K. Jiao, B. Ding and J. Yan, *Advanced Functional Materials*, 2022, **32**, 2201496.